






Article

Potential of Sub-THz-Wave Generation in $\text{Li}_2\text{B}_4\text{O}_7$ Nonlinear Crystal at Room and Cryogenic Temperatures

Dmitry Ezhov ^{1,2,*}, Snezhana Turgeneva ^{3,4}, Nazar Nikolaev ⁵, Alexander Mamrashev ⁵, Sergei Mikerin ³, Fedor Minakov ⁵, Andrey Simanchuk ³, Valery Antsygin ⁵, Valery Svetlichnyi ², Valery Losev ¹ and Yury Andreev ^{1,2,6}

¹ Laboratory of Gas Lasers, Institute of High Current Electronics SB RAS, 634055 Tomsk, Russia; losev@ogl.hcei.tsc.ru (V.L.); yuandreev@yandex.ru (Y.A.)

² Laboratory of Advanced Materials and Technology, National Research Tomsk State University, 634050 Tomsk, Russia; v_svetlichnyi@bk.ru

³ Laboratory of Laser Physics, Institute of Automation and Electrometry SB RAS, 630090 Novosibirsk, Russia; s.turgeneva@g.nsu.ru (S.T.); mikerin@iae.sbras.ru (S.M.); simmk@yandex.ru (A.S.)

⁴ Faculty of Physics, Novosibirsk State University, 630090 Novosibirsk, Russia

⁵ Terahertz Photonics Group, Institute of Automation and Electrometry SB RAS, 630090 Novosibirsk, Russia; nazar@iae.nsk.su (N.N.); mamrashev@iae.nsk.su (A.M.); MinakovFA@iae.nsk.su (F.M.); antsygin@iae.nsk.su (V.A.)

⁶ Laboratory of Geosphere-Biosphere Interactions, Institute of Monitoring of Climatic and Ecological Systems SB RAS, 634055 Tomsk, Russia

* Correspondence: ezhov_dm@phys.tsu.ru; Tel.: +7-3822-531-591



Citation: Ezhov, D.; Turgeneva, S.; Nikolaev, N.; Mamrashev, A.; Mikerin, S.; Minakov, F.; Simanchuk, A.; Antsygin, V.; Svetlichnyi, V.; Losev, V.; et al. Potential of Sub-THz-Wave Generation in $\text{Li}_2\text{B}_4\text{O}_7$ Nonlinear Crystal at Room and Cryogenic Temperatures. *Crystals* **2021**, *11*, 1321. <https://doi.org/10.3390/cryst11111321>

Academic Editor: Shujun Zhang

Received: 23 September 2021

Accepted: 27 October 2021

Published: 29 October 2021

Publisher's Note: MDPI stays neutral with regard to jurisdictional claims in published maps and institutional affiliations.



Copyright: © 2021 by the authors. Licensee MDPI, Basel, Switzerland. This article is an open access article distributed under the terms and conditions of the Creative Commons Attribution (CC BY) license (<https://creativecommons.org/licenses/by/4.0/>).

Abstract: Due to their high optical damage threshold, borate crystals can be used for the efficient nonlinear down-conversion of terawatt laser radiation into the terahertz (THz) frequency range of the electromagnetic spectrum. In this work, we carried out a thorough study of the terahertz optical properties of the lithium tetraborate crystal ($\text{Li}_2\text{B}_4\text{O}_7$; LB4) at 295 and 77 K. Approximating the terahertz refractive index in the form of Sellmeier's equations, we assessed the possibility of converting the radiation of widespread high-power laser sources with wavelengths of 1064 and 800 nm, as well as their second and third harmonics, into the THz range. It was found that four out of eight types of three-wave mixing processes are possible. The conditions for collinear phase matching were fulfilled only for the $o - e \rightarrow o$ type of interaction, while cooling the crystal to 77 K did not practically affect the phase-matching curves. However, a noticeable increase of birefringence in the THz range with cooling (from 0.12 to 0.16) led to an increase in the coherence length for $o - o \rightarrow e$ and $e - e \rightarrow e$ types of interaction, which are potentially attractive for the down-conversion of ultrashort laser pulses.

Keywords: terahertz spectroscopy; lithium tetraborate; temperature dependence; absorption coefficient; refractive index; down-conversion

1. Introduction

A significant development in high-power visible and near-infrared (IR) laser sources has encouraged research into nonlinear media suitable for the efficient conversion of radiation into other spectral ranges [1,2]. One unique case of such a source is the THL-100—a terawatt laser complex generating femtosecond pulses in the visible range. This complex consists of a high-power titanium-sapphire laser, a second harmonic generator, and a gas amplifier operating at the C–A transition in XeF. The THL-100 generates ~30 fs pulses at a wavelength of 475 nm with an energy of up to 1.2 J (corresponding to a peak power of 40 TW) [3]. One promising application of such a laser system is the nonlinear optical generation of intense terahertz pulses (down-conversion) [4]. Several applications of the intense THz waves are intensively developing nowadays. Compact charged particle accelerators could use the benefits of THz radiation (their dimensions limited by the

wavelength of the accelerating electromagnetic field [5,6]). Advances of intense THz generation led to the development of nonlinear optical approaches into new spectral ranges [7]. Moreover, there are a lot of studies on THz waves' selective effect on living organisms [8]. An additionally unsolved problem is the designing and building THz Light Detection and Ranging (LiDAR) system that demands a high-power terahertz source. Since many hazardous industrial and greenhouse gases have absorption lines at sub-terahertz frequencies (where the atmospheric transparency windows are located), such a LiDAR would allow for the monitoring of their small components in the surface layer at kilometer distances for environmental and climatic purposes [9,10].

To achieve the effective down-conversion of intense laser radiation, it is crucial to find nonlinear crystals with a sufficiently large aperture, high optical quality, high damage threshold, and high transparency at pump wavelengths. Nonlinear optical crystals of the borate family satisfy these criteria [11]. Among them, the crystal of lithium tetraborate, $\text{Li}_2\text{B}_4\text{O}_7$ (LB4), has the shortest wavelength of ultraviolet (UV) absorption edge at 0.16 μm , low optical losses ($\alpha \leq 10^{-4} \text{ cm}^{-1}$), and a high damage threshold (up to 40 GW/cm for 10 ns pulses). However, it has lower nonlinear coefficients at a wavelength of 1064 nm ($d_{31} = 0.12 \text{ pm/V}$, $d_{33} = 0.47 \text{ pm/V}$) compared to other borate crystals (β -BBO: $|d_{22}| = 2.2 \text{ pm/V}$; LBO: $|d_{31}| = 0.67 \text{ pm/V}$, $|d_{32}| = 0.85 \text{ pm/V}$) [12]. Nevertheless, these properties make LB4 particularly effective for harmonic generation down to wavelengths near the UV absorption edge [13,14]. These properties also make LB4 a promising converter of UV and visible laser radiation into the THz range using pump intensities near the crystal laser-induced damage threshold. Additionally, the damage threshold and conversion efficiency of the crystal can be increased via cryogenic cooling due to decreases in the absorption of both pump radiation and terahertz waves [15].

Thus, in this work, we studied the terahertz refractive index and absorption coefficient of the lithium tetraborate nonlinear crystal ($\text{Li}_2\text{B}_4\text{O}_7$; LB4) at room (295 K) and liquid nitrogen (77 K) temperatures in the range up to 2 THz. Additionally, we measured and the refractive index and transmission of the crystal in the main transparency window, as well as comparing them with previously published data. The terahertz refractive index was approximated in the form of Sellmeier's equations. The possibility of converting the radiation of widespread high-power laser sources with wavelengths of 1064 and 800 nm, as well as their second (532 and 400 nm) and third (355 and 266 nm) harmonics, into the THz range was assessed. To the best of our knowledge, such thorough studies of terahertz optical properties and possible nonlinear interactions have not previously been carried out.

2. Materials and Methods

The LB4 single crystal was grown in the Institute of Geology and Mineralogy SB RAS, Russia [16]. The samples were plane-parallel plates with a thickness of 350 μm . The plates were polished to optical quality. A dielectric antireflection coating was not applied. The optical z-axis of the samples was placed parallel to the polished surfaces to study optical properties for ordinary and extraordinary waves. The optical properties were measured in both the main transparency window and the terahertz range.

The refractive indices in the main transparency window were measured using a Metricon 2010/M prism coupler system (Metricon Corporation, Pennington, NJ, USA). The operating principle of the system is based on determining the critical angle of laser radiation out-coupling from the measuring prism in the total internal reflection mode. The force of pressing the crystal samples to the prism was 30–40 psi. The system was equipped with five semiconductor lasers with wavelengths of 517.1, 636, 846, 1309.6, and 1547.2 nm, which made it possible to estimate the dispersion of the refractive index of the samples.

The transmission of samples in the visible and IR spectral ranges was investigated by a Cary 5000 spectrophotometer (Varian, Belrose, Australia) with a spectral range of 190–3300 nm and a resolution of 1 nm and by an FT-801 IR Fourier spectrometer (Simex, Novosibirsk, Russia) with a spectral range of 400–4000 cm^{-1} (2.5–25 μm) and a resolution of 2 cm^{-1} .

The terahertz properties were measured using a conventional terahertz time-domain spectrometer (THz-TDS) with a liquid nitrogen bath cryostat. A description of the experimental setup can be found elsewhere [17,18]. In this study, the experimental setup included two smaller diaphragms with apertures of 5 mm due to the small dimensions of the samples under investigation. Additionally, a newly developed measurement procedure described in [19] was applied. This allowed us to measure the absorption coefficient and the refractive index of the crystals for both ordinary and extraordinary waves during one cryostat cooling cycle (without warming up and changing the position of the sample) under nearly the same conditions. THz signals were acquired with a time step of 125 fs in the 60 ps time range, which corresponded to a spectral resolution of about 20 GHz. The temperature expansion coefficient of the LB4 crystal was taken into account when extracting its THz optical properties.

3. Results and Discussion

3.1. Optical Properties in Main Transparency Window

Figure 1a shows the transmission of the LB4 samples in the main transparency window. The crystal was practically transparent up to the wavelength of 3 μm . Then, vibrational absorption bands that are characteristic of the borate structure appeared in the IR range [20,21]. These results are in good agreement with those of prior works [22,23]. The estimated absorption coefficient (see the inset in Figure 1a) was below 0.1 cm^{-1} . Its measurement accuracy was limited by the small thickness of the samples and the noise of the spectrophotometer. The obtained results confirmed the low absorption losses and high optical quality of the samples under study.

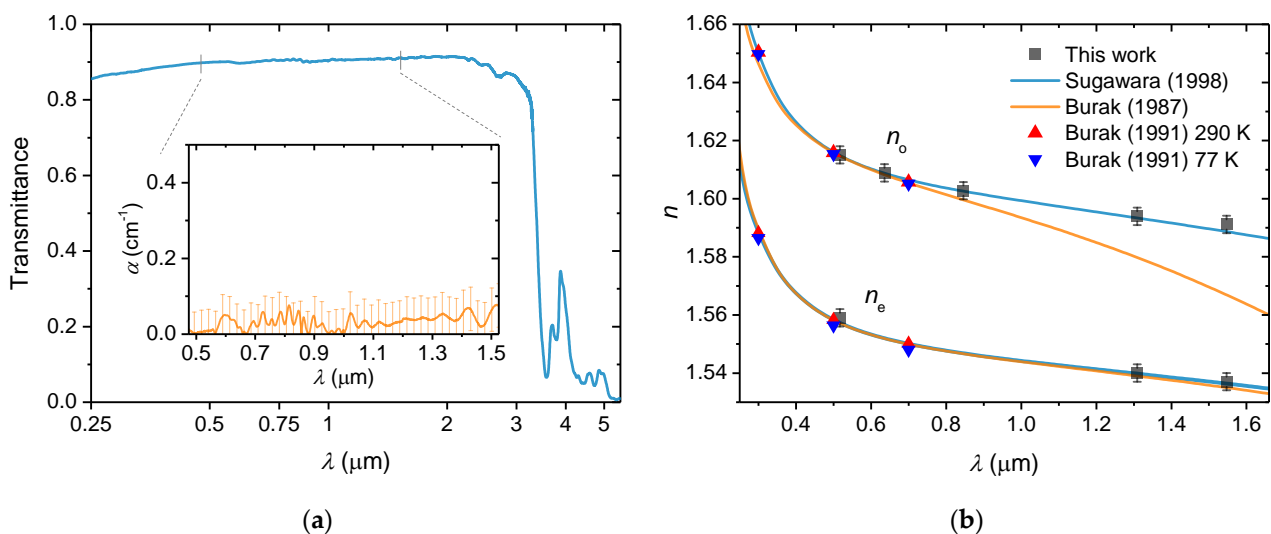


Figure 1. Optical properties in main transparency window: (a) transmittance of LB4 crystal in the visible and infrared regions, measured in non-polarized light; the inset shows an estimate of the absorption coefficient of the sample, taking the dispersion of the reflection coefficient into account. (b) Dispersion of the refractive index of the LB4 crystal for ordinary and extraordinary waves at room temperature (if not specified otherwise).

The refractive index of LB4 was measured at room and higher temperatures in [24,25]. As far as we know, cryogenic measurements have only been presented by Burak et al. [26], and the same data appeared in a review [27]. Burak et al. [25,26] only measured the refractive index in the range of 300–700 nm and approximated it with the Sellmeier equations [26]. This approximation significantly differs in the near-IR range from the Sellmeier equation developed by Sugawara et al. at room temperature [23] (orange and blue curves in Figure 1b). It should also be noted that the high-temperature dependence of the refractive index was investigated via effective nonlinear optical conversion by Umemura et al. [24], but their refined Sellmeier coefficients did not practically differ from those obtained by

Sugawara et al. [23] and were not considered in the current work. The refractive indices we measured (see black squares in Figure 1b and Table 1) are in agreement with the works of Sugawara et al. [23] and Umemura et al. [24].

Table 1. The measured refractive index of the samples.

λ [μm]	n_o	n_e
0.5171	1.61507	1.559
0.636	1.60888	–
0.846	1.60274	–
1.3096	1.5939	1.54
1.5472	1.59114	1.537

It was previously found that the optical and dielectric properties of the LB4 crystal behave discontinuously in the vicinity of 235 K [27,28]. However, we found that the refractive indices at 77 and 290 K did not practically differ [26,27] (as shown by blue and red triangles in Figure 1b, respectively). Thus, for further calculations, we neglected the temperature dependence of the refractive index in the main transparency window and used the Sellmeier equations developed by Umemura et al. [24] for calculations at room and liquid nitrogen temperature.

3.2. Optical Properties in the THz Range

Figure 2 shows absorption coefficients and refractive indices of the crystal measured by the THz-TDS method in the range of 0.5–2 THz at the temperatures of 295 and 77 K. Results below 0.5 THz are not shown since they had low reliability due to the strong diffraction distortions in the 5 mm diaphragm used in the spectrometer and defined by the sample size.

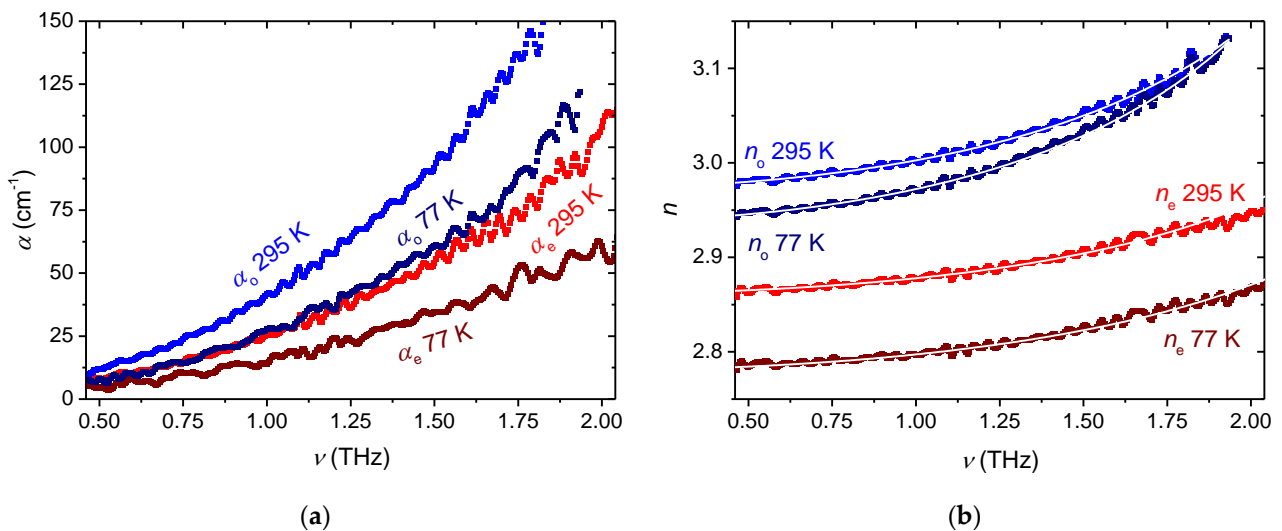


Figure 2. Optical properties of the LB4 crystal in the THz range: (a) Absorption coefficient; (b) dispersion of the refractive index. White lines on top of the experimental data are plotted according to the Sellmeier equation as a visual guide.

It should be noted that the change in the absorption coefficient with cooling (Figure 2a) was not as radical as, for example, that of a lithium triborate (LBO) crystal [29]. Additionally, we considered the contribution of the hopping conductivity of lithium ions to absorption. The dielectric susceptibility peak connected with lithium ion hopping was located at a frequency of about 2.8 GHz at 300 K [28]. Therefore, the absorption coefficient α_e may not drop below 0.1 cm^{-1} even in sub-terahertz frequencies.

The dispersion of the THz refractive index (Figure 2b) also presented peculiarity upon cooling. For example, even though α_o decreased by almost twice in the vicinity of

a frequency of 1.8 THz, n_o did not practically change; however, n_o did change by 0.05 at a frequency of 0.5 THz. The refractive index for the extraordinary wave showed more noticeable changes of ~ 0.08 , which were frequency-independent within the measurement accuracy. These temperature changes were quite small in comparison to the LBO crystal, in which the refractive index of the x -axis n_x changed by ~ 0.24 upon cooling [19].

This behavior of the THz optical properties of the LB4 crystal may be associated with a complex phonon structure and its changes upon cooling [30–32]. For instance, the characteristic shape of the IR absorption spectrum in the region above 150 cm^{-1} shows a large number of absorption bands with a complex temperature behavior [30].

3.3. Assessment of THz-Wave Generation by Down-Conversion

The $\text{Li}_2\text{B}_4\text{O}_7$ compound forms a uniaxial ionic crystal, which belongs to the 4 mm point symmetry group [8]. Its tensor of the second-order nonlinear susceptibility coefficient d_{ij} has the following form [33]:

$$d_{ij} = \begin{pmatrix} 0 & 0 & 0 & 0 & d_{15} & 0 \\ 0 & 0 & 0 & d_{15} & 0 & 0 \\ d_{31} & d_{31} & d_{33} & 0 & 0 & 0 \end{pmatrix}. \quad (1)$$

Within this study, when generating radiation in the THz frequency range, the Kleinman symmetry conditions were not valid because the resulting wave was located behind the infrared absorption band of the crystal. Table 2 provides effective nonlinear coefficients for eight types of three-wave interaction processes possible for THz-wave generation according to [34]. Among these, phase matching for selected wavelengths was only found to be possible for the $o - e \rightarrow o$ type of conversion.

Table 2. Effective nonlinear coefficients for eight possible types of conversion in the LB4 crystal.

Conversion Type	d_{eff}
$o - o \rightarrow o$	0
$o - o \rightarrow e$	$d_{31} \sin \theta$
$o - e \rightarrow o$	$d_{15} \sin \theta$
$o - e \rightarrow e$	0
$e - o \rightarrow o$	$d_{15} \sin \theta$
$e - o \rightarrow e$	0
$e - e \rightarrow o$	0
$e - e \rightarrow e$	$(2d_{15} + d_{31}) \cos^2 \theta \sin \theta + d_{33} \sin^3 \theta$

In order to evaluate coherence lengths and phase-matching curves for these types of conversion, we approximated the dispersion of the refractive index for the THz range in the form of Sellmeier equations. It should be mentioned that a Sellmeier equation usually contains information about the frequency of the absorption peak (in the general case of the short-wavelength edge). However, due to the complex phonon structure of the crystal at frequencies above 2.5 THz, additional terms in the equation significantly complicated it and were omitted. Equations (2) and (3) are simplified approximations of the THz refractive index at room (2) and liquid nitrogen (3) temperature:

$$n_o^2 = 7.31 + \frac{1.53\lambda^2}{\lambda^2 - 9276}, \quad n_e^2 = 7.304 + \frac{0.883\lambda^2}{\lambda^2 - 8734}. \quad (2)$$

$$n_o^2 = 6.98 + \frac{1.65\lambda^2}{\lambda^2 - 9912}, \quad n_e^2 = 6.67 + \frac{1.06\lambda^2}{\lambda^2 - 7327}. \quad (3)$$

The approximations made well fits the experimental data (white curves in Figure 2b). The refractive indices n_o and n_e for the pump radiation in the main transparency window were approximated using the expressions proposed by Umemura et al. [24] for both

295 and 77 K, since it was shown above that they only slightly differed for these two temperature points.

For the types of three-wave interaction with a collinear propagation, the efficiency of which is not identically equal to zero, we carried out a numerical simulation of the coherence length:

$$L_c = \pi \times [k(\lambda_{\text{pump}_1}) - k(\lambda_{\text{pump}_2}) - k(\lambda_{\text{pump}_3})]^{-1}, \quad (4)$$

where $k(\lambda) = 2\pi n(\lambda)/\lambda$; $1/\lambda_{\text{pump}_1} - 1/\lambda_{\text{pump}_2} = 1/\lambda_{\text{diff}}$, λ_{pump_1} , and λ_{pump_2} are the pump radiation wavelengths; and λ_{diff} is the resulting THz wavelength. A simulation was carried out for two temperatures of 295 and 77 K. Results are shown in Figure 3. From the dependence of L_c on the angle θ for fixed pump and difference wavelengths (Figure 3a), it can be seen that phase matching existed only for the $o - e \rightarrow o$ conversion type. However, the $o - o \rightarrow e$ and $e - e \rightarrow e$ types are also worth noting since their coherence lengths were found to weakly depend on θ . Figure 3a also demonstrates small differences in the coherence lengths for room and cryogenic temperatures. Figure 3b shows the phase-matching curves of the $o - e \rightarrow o$ conversion type when LB4 was pumped at the wavelengths of widespread high-power laser sources (1064 and 800 nm) and their second and third harmonics.

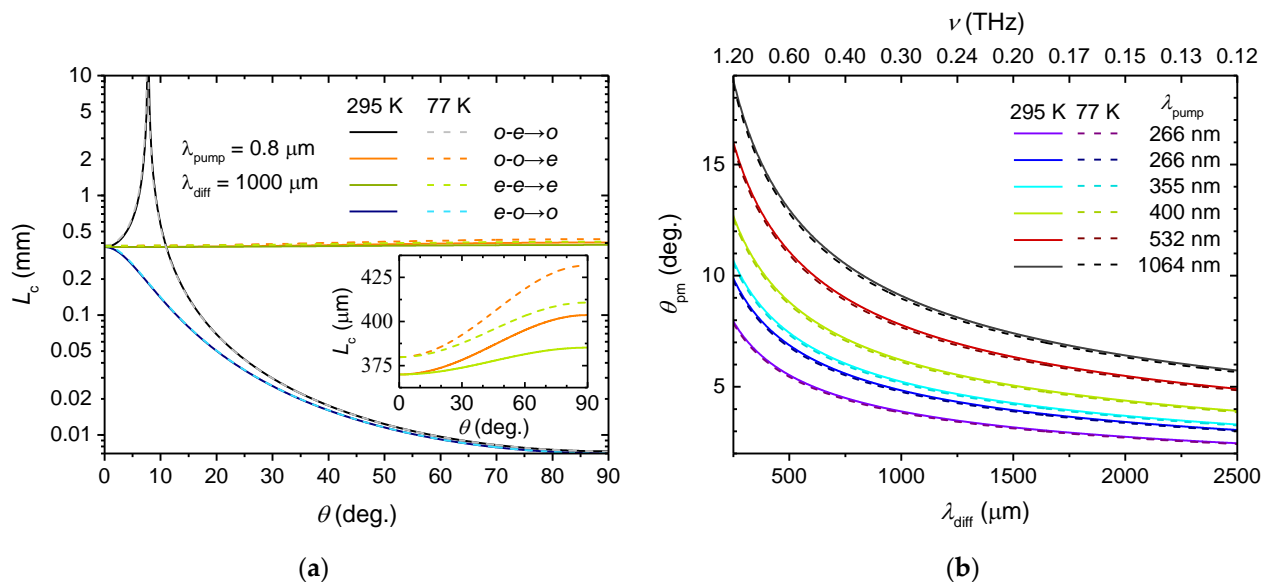


Figure 3. Phase-matching simulation: (a) dependence of the coherence length on the angle θ for four conversion types that resulted in THz wave generation in LB4. Pump wavelengths were in the vicinity of $0.8 \mu\text{m}$, and the resulting wavelength was $1000 \mu\text{m}$ (0.3 THz). The inset shows an enlarged dependence for the $o - o \rightarrow e$ and $e - e \rightarrow e$ conversions types. (b) Phase-matching curves for the $o - e \rightarrow o$ conversion of various pump wavelengths to the sub-THz range.

It follows from Figure 3b that cooling down the crystal from 295 to 77 K had practically no effect on the phase-matching curves. It should also be noted that for higher harmonics of pump radiation, a smaller phase-matching angle θ_{pm} is required. This is a fairly negative factor since it leads to a decrease in d_{eff} proportional to $\sin(\theta)$. However, an increase in the d_{15} coefficient with a decrease of the wavelength can partially compensate for this. An estimate of the d_{15} in accordance with Miller's rule [35] provided an increase of its value by $\sim 18\%$ as the pump wavelength decreased from 1064 to 266 nm. As a result, according to our estimates, the resulting decrease in d_{eff} was only about 50%.

Let us consider other types of conversion without phase matching but with non-zero effective nonlinearity. Since a coherence length of several hundred microns is sufficient for efficient nonlinear frequency conversion, it is of interest to use this crystal with high-power femtosecond sources. The coherence lengths for the $o - o \rightarrow e$ and $e - e \rightarrow e$ types were

found to be practically independent of the angle θ . In this case, it was advisable to take such an angle θ for which d_{eff} was maximal. For the $o-o \rightarrow e$ conversion, the angles were $\theta = \pm 90^\circ$. However, the picture was more complicated for the $e-e \rightarrow e$ type, as $d_{\text{eff}}^{e-e \rightarrow e}$ consisted of two terms (Table 2). The first one was proportional to $\sin^3(\theta)$, which reached the maximum value at the angle $\theta = \pm 90^\circ$. The second term was proportional to $\cos^2(\theta) \sin(\theta)$, which was maximal at $\theta = \pm 35.26^\circ$. Thus, the efficiency depended on the values of the coefficients d_{15} , d_{31} , and d_{33} , which had to be experimentally determined in the THz region. However, for further estimates, we assumed that the ratio of these coefficients for the types of conversion that resulted in terahertz frequency generation approximately equaled their ratio for the main transparency window of the crystal, i.e., $d_{31} \approx d_{15}$ and $d_{33}/d_{15} \approx 4$. In this case, the term proportional to $\sin^3(\theta)$ dominated, and the maximum for $d_{\text{eff}}^{e-e \rightarrow e}$ occurred for the values of the angle $\theta = \pm 90^\circ$.

Figure 4 shows the dependence of the coherence length on the pump wavelength for the $o-o \rightarrow e$ and $e-e \rightarrow e$ conversion types at $\theta = \pm 90^\circ$; $\lambda_{\text{diff}} = 1000 \mu\text{m}$ and $3000 \mu\text{m}$ were used for the sake of estimation.

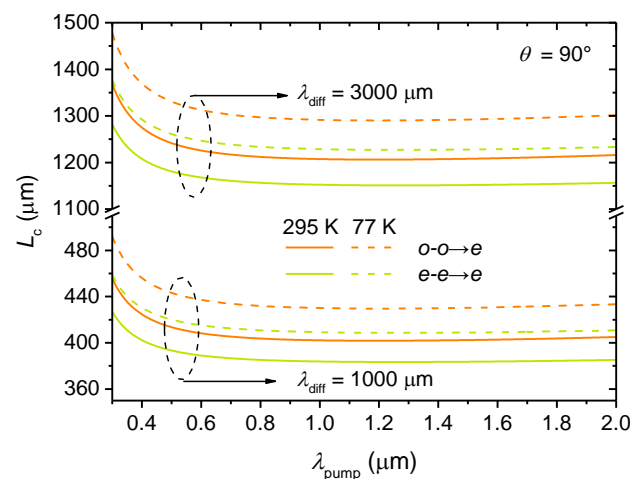


Figure 4. Dependence of the coherence length on the pump wavelength for the $o-o \rightarrow e$ and $e-e \rightarrow e$ conversion types that generate radiation at the wavelengths of 1000 and 3000 μm .

One can see that for a fixed generated wavelength λ_{diff} , the coherence length L_c also weakly depended on the pump frequency, except for a small increase in the short-wavelength region. Thus, the use of short pump wavelengths for the generation of sub-THz radiation may be efficient because of both an increase in the quadratic susceptibility of the crystal and a small increase in the coherence length. Cooling the crystal from 295 to 77 K also led to a small growth of L_c . In general, a crystal with a thickness of at least 370 μm can be used to generate millimeter wavelengths $\lambda_{\text{diff}} > 1 \text{ mm}$ ($\nu < 300 \text{ GHz}$) in the transparency window of the atmosphere.

4. Conclusions

Conducted analyses, experimental studies, and calculations showed that cooling of the LB4 crystal from room to liquid nitrogen temperature did not practically affect its refractive index in the main transparency window. At the same time, in the THz range, a significant decrease of absorption was observed for both ordinary and extraordinary waves. However, unlike LBO, absorption in LB4 did not decrease to a “zero” level at 77 K due to the peculiarities of the crystal structure. The THz refractive index n_e demonstrated the highest temperature dependence that led to an increase in birefringence $\Delta n = n_o - n_e$ by more than 30% at 77 K.

The evaluation of the possibility of generating THz radiation from high-power sources of the visible and near-IR range (operating in the main transparency window of LB4) via down-conversion showed that only four out of eight types of conversion are possible (they

were found to have non-zero nonlinear coefficients). Phase-matching conditions were only fulfilled for the $o - e \rightarrow o$ conversion type. At the same time, the coherence length for the $o - o \rightarrow e$ and $e - e \rightarrow e$ types of interaction were estimated at several hundred microns, which is sufficient for efficient conversion when using high-power femtosecond lasers when taking the high damage threshold of LB4 into account. We suppose that cooling the crystal should increase conversion efficiency due to a decrease in the absorption losses of the pump and the THz waves, as well as a slight increase in the coherence length.

Therefore, our study has shown the potential efficiency and provided the necessary conditions for the nonlinear generation of THz radiation in an LB4 crystal pumped by widespread high-power lasers with wavelengths of 1064 and 800 nm, as well as their harmonics.

Author Contributions: Conceptualization and supervision, Y.A.; investigation, D.E., S.T., S.M. and A.S.; writing—original draft, D.E. and N.N.; visualization, D.E. and N.N.; data curation, N.N. and V.A.; software, A.M. and F.M.; writing—review and editing, A.M. and V.S.; methodology, A.M.; resources, V.A.; validation, V.S.; funding acquisition and project administration, V.L. All authors have read and agreed to the published version of the manuscript.

Funding: The research was funded by the Russian Science Foundation, project № 19–19–00241.

Data Availability Statement: Not applicable.

Acknowledgments: The authors acknowledge the Shared Equipment Center “Spectroscopy and Optics” of the Institute of Automation and Electrometry SB RAS providing the terahertz time-domain spectrometer and Metricon system.

Conflicts of Interest: The authors declare no conflict of interest. The funders had no role in the design of the study; in the collection, analyses, or interpretation of data; in the writing of the manuscript, or in the decision to publish the results.

References

1. Huang, S.-W.; Granados, E.; Huang, W.R.; Hong, K.-H.; Zapata, L.E.; Kärtner, F.X. High Conversion Efficiency, High Energy Terahertz Pulses by Optical Rectification in Cryogenically Cooled Lithium Niobate. *Opt. Lett.* **2013**, *38*, 796–798. [[CrossRef](#)]
2. Wu, M.-H.; Tsai, W.-C.; Chiu, Y.-C.; Huang, Y.-C. Generation of ~ 100 KW Narrow-Line Far-Infrared Radiation from a KTP off-Axis THz Parametric Oscillator. *Optica* **2019**, *6*, 723–730. [[CrossRef](#)]
3. Alekseev, S.V.; Ivanov, N.G.; Losev, V.F.; Mesyats, G.A.; Mikheev, L.D.; Ratakhin, N.A.; Panchenko, Y.N. THL-100 Multi-Terawatt Laser System of Visible Spectrum Range. *Opt. Commun.* **2020**, *455*, 124386. [[CrossRef](#)]
4. Lubenko, D.M.; Losev, V.F.; Ezhov, D.M.; Andreev, Y.M.; Lanskiy, G.V.; Lisenko, A.A. Generation of High Power THz Radiation in ZnGeP₂ upon Femtosecond Ti:Sapphire Laser Pumping. *Bull. Russ. Acad. Sci. Phys.* **2020**, *84*, 1039–1042. [[CrossRef](#)]
5. Tang, H.; Zhao, L.; Zhu, P.; Zou, X.; Qi, J.; Cheng, Y.; Qiu, J.; Hu, X.; Song, W.; Xiang, D.; et al. Stable and Scalable Multistage Terahertz-Driven Particle Accelerator. *Phys. Rev. Lett.* **2021**, *127*, 074801. [[CrossRef](#)] [[PubMed](#)]
6. Nanni, E.A.; Huang, W.R.; Hong, K.-H.; Ravi, K.; Fallahi, A.; Moriena, G.; Dwayne Miller, R.J.; Kärtner, F.X. Terahertz-Driven Linear Electron Acceleration. *Nat. Commun.* **2015**, *6*, 8486. [[CrossRef](#)] [[PubMed](#)]
7. Hafez, H.A.; Kovalev, S.; Tielrooij, K.; Bonn, M.; Gensch, M.; Turchinovich, D. Terahertz Nonlinear Optics of Graphene: From Saturable Absorption to High-Harmonics Generation. *Adv. Opt. Mater.* **2020**, *8*, 1900771. [[CrossRef](#)]
8. Cherkasova, O.P.; Serdyukov, D.S.; Ratushnyak, A.S.; Nemova, E.F.; Kozlov, E.N.; Shidlovskii, Y.V.; Zaytsev, K.I.; Tuchin, V.V. Effects of Terahertz Radiation on Living Cells: A Review. *Opt. Spectrosc.* **2020**, *128*, 855–866. [[CrossRef](#)]
9. Bigourd, D.; Cuisset, A.; Hindle, F.; Matton, S.; Fertein, E.; Bocquet, R.; Mouret, G. Detection and Quantification of Multiple Molecular Species in Mainstream Cigarette Smoke by Continuous-Wave Terahertz Spectroscopy. *Opt. Lett.* **2006**, *31*, 2356–2358. [[CrossRef](#)]
10. Hsieh, Y.-D.; Nakamura, S.; Abdelsalam, D.G.; Minamikawa, T.; Mizutani, Y.; Yamamoto, H.; Iwata, T.; Hindle, F.; Yasui, T. Dynamic Terahertz Spectroscopy of Gas Molecules Mixed with Unwanted Aerosol under Atmospheric Pressure Using Fibre-Based Asynchronous-Optical-Sampling Terahertz Time-Domain Spectroscopy. *Sci. Rep.* **2016**, *6*, 28114. [[CrossRef](#)]
11. Chen, C.; Sasaki, T.; Li, R.; Wu, Y.; Lin, Z.; Mori, Y.; Hu, Z.; Wang, J.; Uda, S.; Yoshimura, M.; et al. *Nonlinear Optical Borate Crystals, Principles and Applications*; Wiley-VCH: Weinheim, Germany, 2012. [[CrossRef](#)]
12. Nikogosyan, D.N. *Nonlinear Optical Crystals: A Complete Survey*; Springer: New York, NY, USA, 2005. [[CrossRef](#)]
13. Komatsu, R.; Sugawara, T.; Sassa, K.; Sarukura, N.; Liu, Z.; Izumida, S.; Segawa, Y.; Uda, S.; Fukuda, T.; Yamanouchi, K. Growth and Ultraviolet Application of Li₂B₄O₇ Crystals: Generation of the Fourth and Fifth Harmonics of Nd:Y₃Al₅O₁₂ Lasers. *Appl. Phys. Lett.* **1997**, *70*, 3492–3494. [[CrossRef](#)]

14. Suzuki, Y.; Ono, S.; Murakami, H.; Kozeki, T.; Ohtake, H.; Sarukura, N.; Masada, G.; Shiraishi, H.; Sekine, I. 0.43 J, 10 Hz Fourth Harmonic Generation of Nd:YAG Laser Using Large $\text{Li}_2\text{B}_4\text{O}_7$ Crystals. *Jpn. J. Appl. Phys.* **2002**, *41*, 68–70. [[CrossRef](#)]
15. Wu, X.; Zhou, C.; Huang, W.R.; Ahr, F.; Kärtner, F.X. Temperature Dependent Refractive Index and Absorption Coefficient of Congruent Lithium Niobate Crystals in the Terahertz Range. *Opt. Express* **2015**, *23*, 29729. [[CrossRef](#)]
16. Antsygin, V.D.; Mamrashev, A.A.; Nikolaev, N.A.; Potaturkin, O.I.; Bekker, T.B.; Solntsev, V.P. Optical Properties of Borate Crystals in Terahertz Region. *Opt. Commun.* **2013**, *309*, 333–337. [[CrossRef](#)]
17. Rybak, A.; Antsygin, V.; Mamrashev, A.; Nikolaev, N. Terahertz Optical Properties of KTiOPO_4 Crystal in the Temperature Range of (−192)–150 °C. *Crystals* **2021**, *11*, 125. [[CrossRef](#)]
18. Wang, C.R.; Pan, Q.K.; Chen, F.; Lanski, G.; Nikolaev, N.; Mamrashev, A.; Andreev, Y.; Meshalkin, A. Phase-Matching in KTP Crystal for THz Wave Generation at Room Temperature and 81 K. *Infrared Phys. Technol.* **2019**, *97*, 1–5. [[CrossRef](#)]
19. Mamrashev, A.; Minakov, F.; Nikolaev, N.; Antsygin, V. Terahertz Time-Domain Polarimetry for Principal Optical Axes of Anisotropic Crystals. *Photonics* **2021**, *8*, 213. [[CrossRef](#)]
20. Jun, L.; Shuping, X.; Shiyang, G. FT-IR and Raman Spectroscopic Study of Hydrated Borates. *Spectrochim. Acta Part A Mol. Biomol. Spectrosc.* **1995**, *51*, 519–532. [[CrossRef](#)]
21. Kwon, T.Y.; Ju, J.J.; Cha, J.W.; Kim, J.N.; Yun, S.I. Characteristics of Critically Phase-Matched Second-Harmonic Generation of a $\text{Li}_2\text{B}_4\text{O}_7$ Crystal Grown by the Czochralski Method. *Mater. Lett.* **1994**, *20*, 211–215. [[CrossRef](#)]
22. Shiro, Y.; Komatsu, R.; Fujino, S. Influence of Scattering Centers on UV Transmittance in $\text{Li}_2\text{B}_4\text{O}_7$ Single Crystals and Its Origin. *Trans. Mater. Res. Soc. Jpn.* **2007**, *32*, 729–732. [[CrossRef](#)]
23. Sugawara, T.; Komatsu, R.; Satoshi, U.; Uda, S. Linear and Nonlinear Optical Properties of Lithium Tetraborate. *Solid State Commun.* **1998**, *107*, 233–237. [[CrossRef](#)]
24. Umemura, N.; Watanabe, J.; Matsuda, D.; Kamimura, T. Refined Sellmeier and Thermo-Optic Dispersion Formulas for $\text{Li}_2\text{B}_4\text{O}_7$. *Jpn. J. Appl. Phys.* **2017**, *56*, 032602. [[CrossRef](#)]
25. Burak, Y.V.; Gitskailo, G.M.; Lyseiko, I.T.; Pidzyrailo, N.S.; Stefansky, I.V. Temperaturnaya Zavisimost Pokazatelya Prelomleniya Kristallov $\text{Li}_2\text{B}_4\text{O}_7$. *Ukr. Fiz. Zh.* **1987**, *32*, 1509–1510. (In Russian)
26. Burak, Y.V.; Gaba, V.M.; Lyseiko, I.T.; Romanyuk, N.A.; Stadnik, V.I.; Stefansky, I.V.; Ursul, Z.M. Temperaturnaya i Spectralnaya Zavisimosti Pokazatelya Prelomleniya Monokristallov Tetraborata Litiya. *Ukr. Fiz. Zh.* **1991**, *36*, 1638–1642. (In Russian)
27. Gorelik, V.S.; Vdovin, A.V.; Moiseenko, V.N. Raman and Hyper-Rayleigh Scattering in Lithium Tetraborate Crystals. *J. Russ. Laser Res.* **2003**, *24*, 553–605. [[CrossRef](#)]
28. Akishige, Y.; Komatsu, R. Peculiar Dielectric Behaviors on $\text{Li}_2\text{B}_4\text{O}_7$ Single Crystals. *J. Phys. Soc. Jpn.* **2004**, *73*, 1341–1346. [[CrossRef](#)]
29. Nikolaev, N.A.; Andreev, Y.M.; Kononova, N.G.; Mamrashev, A.A.; Antsygin, V.D.; Kokh, K.A.; Kokh, A.E.; Losev, V.F.; Potaturkin, O.I. Terahertz Optical Properties of LBO Crystal upon Cooling to Liquid Nitrogen Temperature. *Quantum Electron.* **2018**, *48*, 19–21. [[CrossRef](#)]
30. Zhigadlo, N.D.; Zhang, M.; Salje, E.K.H. An Infrared Spectroscopic Study of $\text{Li}_2\text{B}_4\text{O}_7$. *J. Phys. Condens. Matter* **2001**, *13*, 6551–6561. [[CrossRef](#)]
31. Elbelrhiti Elalaoui, A.; Maillard, A.; Fontana, M.D. Raman Scattering and Non-Linear Optical Properties in $\text{Li}_2\text{B}_4\text{O}_7$. *J. Phys. Condens. Matter* **2005**, *17*, 7441–7454. [[CrossRef](#)]
32. Vdovin, A.V.; Moiseenko, V.N.; Burak, Y.V. Vibrational Spectrum of $\text{Li}_2\text{B}_4\text{O}_7$ Crystals. *Opt. Spectrosc.* **2001**, *90*, 555–560. [[CrossRef](#)]
33. Powers, P.E. *Field Guide to Nonlinear Optics*; SPIE Press: Bellingham, WA, USA, 2013. [[CrossRef](#)]
34. Boyd, G.D.; Kleinman, D.A. Parametric Interaction of Focused Gaussian Light Beams. *J. Appl. Phys.* **1968**, *39*, 3597–3639. [[CrossRef](#)]
35. Miller, R.C. Optical Second Harmonic Generation in Piezoelectric Crystals. *Appl. Phys. Lett.* **1964**, *5*, 17–19. [[CrossRef](#)]